

Defect configurations and dynamical behavior in a Gay-Berne nematic emulsion

Jeffrey L. Billeter and Robert A. Pelcovits

Department of Physics, Brown University, Providence, Rhode Island 02912

(Received 23 November 1999)

To model a nematic emulsion consisting of a surfactant-coated water droplet dispersed in a nematic host, we performed a molecular dynamics simulation of a droplet immersed in a system of 2048 Gay-Berne ellipsoids in a nematic phase. Strong radial anchoring at the surface of the droplet induced a Saturn ring defect configuration, consistent with theoretical predictions for very small droplets. A surface ring configuration was observed for lower radial anchoring strengths, and a pair of point defects was found near the poles of the droplet for tangential anchoring. We also simulated the falling ball experiment and measured the drag force anisotropy, in the presence of strong radial anchoring as well as zero anchoring strength.

PACS number(s): 61.30.Jf, 64.70.Md, 61.30.Cz

I. INTRODUCTION

With a wide variety of practical applications and numerous opportunities for investigating basic questions in chemistry and physics, colloidal systems (suspensions of solid particles) and emulsions (dispersions of surfactant-coated liquid droplets) are of great interest to a variety of researchers. Recently, there has been increased attention given to emulsions involving water droplets dispersed in liquid crystals [1]. Surfactant-coated water droplets dispersed in a nematic host (so-called inverted emulsions, as opposed to direct emulsions, where the nematic itself is separated into spherical droplets) can serve as generators of topological defects because of the anchoring of the liquid crystalline molecules to the droplet surfaces. Sufficiently strong homeotropic anchoring at the surface of the droplet induces a radial hedgehog defect centered on the droplet. To compensate for this induced defect, another defect must be created in the medium.

There are two defect configurations which are theorized to arise in this case—the hyperbolic dipole [2] and the Saturn ring [3] (see Fig. 1). In the dipole case, the radial hedgehog defect is compensated by another point defect (a hyperbolic hedgehog); the two together form the dipole. The Saturn ring is a hyperbolic wedge disclination line which encircles the droplet equatorially. At large distances, the Saturn ring has the appearance of a hyperbolic hedgehog. In both cases then, the radial hedgehog with defect index $+1$ is compensated for by a hyperbolic defect with index -1 . Note that in the dipole case, the line joining the droplet and the hyperbolic monopole is parallel to the director $\hat{\mathbf{n}}$, while in the Saturn ring case, the normal to the plane of the ring is parallel to $\hat{\mathbf{n}}$. Theoretical and numerical work based on elastic theory [2,3,5,7] suggested that the dipole configuration is stable for micron sized droplets and sufficiently strong surface anchoring, while a Saturn ring should appear if the droplet size is reduced. If the strength of the surface anchoring is reduced, a third director configuration can arise, termed the surface-ring configuration [4–6]. In this configuration the molecules at the equator are actually parallel to the droplet's surface (homotropic), and radial anchoring is limited to the poles of the droplet. Experiments to date have always revealed dipolar

configurations [1], consistent with the relatively large particle sizes and surface anchoring used. Changing the surfactant compound to produce homotropic (tangential) anchoring at the surface results in a pair of point defects at the poles of the droplet (boojums).

The dynamics of the dispersed droplets and their accompanying director configurations are also of interest [4,8]. A detailed knowledge of the flow properties of liquid crystals is important for both fundamental and technological reasons. One way to measure viscosities in a fluid is via the “falling ball experiment.” The drag force on a falling ball can be related to the viscosity by a Stokes-type formula $F_d = -6\pi Rv\eta$, where R is the radius of the ball, v is its terminal velocity, and η is the fluid viscosity. Because of the anisotropy of liquid crystalline molecules, the drag force on a moving water droplet in an inverse nematic emulsion will depend on the relative orientation of the velocity and the director, i.e., a Stokes-like formula incorporates a nematic resistance tensor M [4,8],

$$\mathbf{F} = M_{\perp} \mathbf{v} + (M_{\parallel} - M_{\perp})(\mathbf{v} \cdot \hat{\mathbf{n}})\hat{\mathbf{n}}, \quad (1)$$

where the subscripts \perp and \parallel refer to directions perpendicular and parallel to the director, respectively. Equation (1) implies that the drag force will not be antiparallel to the velocity, but will instead have a component F_{lift} perpendicular to \mathbf{v} . The drag force is particularly sensitive to the defect structure around the droplet, because regions of high gradients in the director field (such as those around defects) result in higher resistance to flow. Theoretical work on the drag force exerted on spheres as well as cylinders was carried out by Ruhwandl and Terentjev [4,8] in the low Ericksen number regime (small values of $vR\eta/K$, where v and R are the droplet velocity and radius, respectively, and η and K are characteristic values of the nematic viscosity and elastic constant respectively) where they found a drag force anisotropy (the ratio F_{\perp}/F_{\parallel}) in the range of 1.5–1.75. A drag force anisotropy not equal to unity is equivalent to a nonzero lift force. These authors also considered discotic molecules [8], and found a ratio less than unity which is reasonable given the oblate shape of the molecule.

Here we present the results of molecular dynamics (MD) simulations carried out on a system consisting of one spheri-

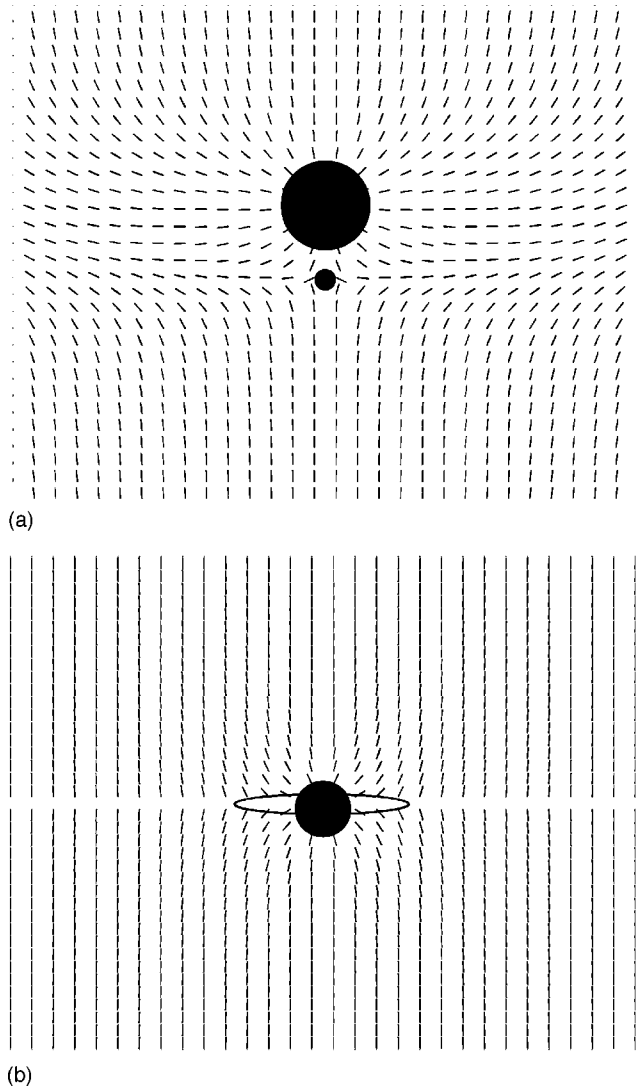


FIG. 1. Two possible defect configurations surrounding a water droplet placed in a nematic host, with strong radial surface anchoring. The droplet is indicated by the large sphere. (a) Dipole configuration showing the induced hyperbolic monopole, indicated by the small sphere. (b) Saturn ring consisting of an induced wedge disclination ring about the droplet. The Saturn ring extends into and out of the plane of the page.

cal droplet immersed in a Gay-Berne nematic liquid crystal [9]. The Gay-Berne model is a phenomenological single site model of mesogenic molecules which captures the essential physical features of a wide variety of liquid crystalline behavior [10]. Using a fluid model like the Gay-Berne system, as opposed to a lattice model of liquid crystals, we are able to simulate not only static behavior such as the director configuration surrounding the sphere (including the role of thermal fluctuations which are neglected in elastic theory), but dynamical behavior as well. We model the interaction of the Gay-Berne molecules with the droplet using a generalized repulsive Gay-Berne potential [11] to account for excluded volume effects along with a phenomenological surface anchoring potential. Due to the large computational overhead of the Gay-Berne system, our study is restricted to 2048 Gay-Berne particles and a relatively small droplet, with a diameter equal to the long axis of the Gay-Berne molecule.

However, using massively parallel computers it is possible to study much larger Gay-Berne systems consisting of at least 65 000 molecules [12,13], and we hope to carry out a simulation of the emulsion system with a similar number of host molecules in the future.

The outline of this paper is as follows. In Sec. II we present the computational details of our study. Section III contains the results for the director configuration in the absence of an external force on the droplet, as well as the results of ‘falling ball’ type experiments. We offer some concluding remarks in Sec. IV.

II. COMPUTATIONAL DETAILS

We model the nematic host using the original Gay-Berne potential given by [14]

$$U(\hat{\mathbf{u}}_i, \hat{\mathbf{u}}_j, \hat{\mathbf{r}}) = 4\varepsilon(\hat{\mathbf{u}}_i, \hat{\mathbf{u}}_j, \hat{\mathbf{r}}) \left[\left\{ \frac{\sigma_0}{r - \sigma(\hat{\mathbf{u}}_i, \hat{\mathbf{u}}_j, \hat{\mathbf{r}}) + \sigma_0} \right\}^{12} - \left\{ \frac{\sigma_0}{r - \sigma(\hat{\mathbf{u}}_i, \hat{\mathbf{u}}_j, \hat{\mathbf{r}}) + \sigma_0} \right\}^6 \right], \quad (2)$$

where $\hat{\mathbf{u}}_i$ and $\hat{\mathbf{u}}_j$ give the orientations of the long axes of molecules i and j , respectively, and \mathbf{r} is the intermolecular vector ($\mathbf{r} = \mathbf{r}_i - \mathbf{r}_j$). The parameter $\sigma(\hat{\mathbf{u}}_i, \hat{\mathbf{u}}_j, \hat{\mathbf{r}})$ is the intermolecular separation at which the potential vanishes, and thus represents the shape of the molecules. The well depth $\varepsilon(\hat{\mathbf{u}}_i, \hat{\mathbf{u}}_j, \hat{\mathbf{r}})$ represents the anisotropy of the attractive interactions. The explicit form of these functions was given in Ref. [14]. For the adjustable parameters appearing in these functions, we primarily used the values originally proposed by Gay and Berne [9]. We also ran simulations with the parameterization suggested by Berardi *et al.* [15], and saw no noticeable differences in our results.

The interaction between the Gay-Berne molecules and a droplet of radius R consists of two parts—a soft, repulsive term U_r and an anchoring term U_a . The repulsive term utilizes the parameters of a Gay-Berne potential generalized to mimic the interaction between nonequivalent particles [11]. The range parameter $\sigma_r(\hat{\mathbf{u}}, \hat{\mathbf{r}})$ and the energy parameter $\varepsilon_r(\hat{\mathbf{u}})$ used in this potential are generalizations of the corresponding parameters in Eq. (2), namely,

$$\sigma_r(\hat{\mathbf{u}}, \hat{\mathbf{r}}) = \sigma_o^r [1 - \chi_r(\hat{\mathbf{r}} \cdot \hat{\mathbf{u}})]^{-1/2} \quad (3)$$

and

$$\varepsilon_r(\hat{\mathbf{u}}, \hat{\mathbf{r}}) = 1, \quad (4)$$

with χ_r defined as

$$\chi_r = \frac{\sigma_e^2 - \sigma_o^2}{\sigma_e^2 + 4R^2}, \quad (5)$$

and

$$\sigma_o^r = \frac{1}{\sqrt{2}} (\sigma_o^2 + 4R^2)^{1/2}. \quad (6)$$

The parameters σ_o and σ_e are the values of $\sigma(\hat{\mathbf{u}}_i, \hat{\mathbf{u}}_j, \hat{\mathbf{r}})$ when the two molecules are oriented side by side and end to end respectively. Thus the repulsive part of the potential between a molecule with orientation $\hat{\mathbf{u}}$ and the droplet with center of mass separation \mathbf{r} is given by

$$U_r(\hat{\mathbf{u}}, \hat{\mathbf{r}}) = 4\varepsilon_o \left\{ \frac{\sigma_o}{r - \sigma_r(\hat{\mathbf{u}}, \hat{\mathbf{r}}) + \sigma_o} \right\}^{18}, \quad (7)$$

where the overall energy scale is set by ε_o . We use an exponent of 18 instead of 12 in this repulsive term to make the interaction ‘‘harder.’’

The short-ranged surface anchoring term is given by

$$U_a = -W \frac{(\hat{\mathbf{r}} \cdot \hat{\mathbf{u}})^6}{r^6}, \quad (8)$$

where W is a phenomenological anchoring coefficient. Only those molecules with $r < R + \sigma_e$ are considered to interact with the droplet via this surface anchoring. A positive value of W yields homeotropic anchoring, while a negative value of W gives tangential anchoring.

We performed MD simulations at a constant temperature $T^* \equiv k_B T / \varepsilon_o = 0.95$ and constant pressure, $P^* = P \sigma_o^3 / \varepsilon_o = 4.0$, corresponding to a nematic phase. We controlled temperature and pressure using the equations of motion of Refs. [16] and [17], which are modifications of the original Nose-Hoover approach [18]. The orientational degrees of freedom were parametrized using quaternions. We used a variation [19] of the leapfrog algorithm to solve these equations for a system consisting of 2048 Gay-Berne molecules and one spherical droplet with a time step $\Delta t^* = 0.001$ and $\Delta t^* \equiv (m \sigma_o^2 / \varepsilon_o)^{-1/2}$, where m is the mass of the Gay-Berne molecule. The droplet diameter was chosen to be $3\sigma_o$, which is the length of the long axis of the Gay-Berne molecules in the host, and the mass of the droplet was chosen to be $100m$, so that in the absence of an external force the sphere moves very slowly compared to the molecules. The surface anchoring parameter W was chosen to be 4000 (in dimensionless units) for weak anchoring and 35000 for strong anchoring. In terms of the dimensionless quantity $\xi = K / WR$, which measures the elastic deformation energy relative to the surface anchoring energy [20], the former value of W corresponds to $\xi \approx 0.4$, while the latter corresponds to a value of ξ ten times smaller (these values assume that K is of order unity). We prepared our system by placing the sphere at the center of an empty MD cell. We then surrounded the sphere with eight replicas of a Gay-Berne nematic phase of 256 particles, equilibrated to the temperature and pressure specified above. The system was then equilibrated for 100000 time steps. For our system of 2048 particles, approximately 100 are subject to the short-range surface anchoring energy [Eq. (8)]. For weak anchoring we found a nematic order parameter $S = 0.68$, compared with a value of 0.69 in the absence of the sphere. The total surface anchoring energy for small W accounts for about 2% of the total potential energy. For strong anchoring we found $S = 0.64$, and a total surface energy that was 29% of the total.

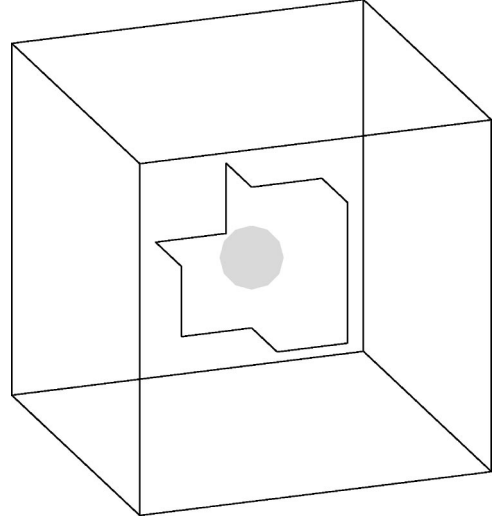


FIG. 2. A Saturn ring surrounding the droplet (of diameter $3\sigma_o$) at the center of the MD cell, with surface anchoring parameter $W = 35000$ (strong anchoring). The ring was located using the disclination-finding algorithm described in [21]. The MD cell was divided into a $6 \times 6 \times 6$ lattice, leading to the jagged appearance of the ring. Most of the ring segments are located in the equatorial plane perpendicular to the director.

III. RESULTS

A. Static director configuration

In the absence of an external force on the droplet we studied the director configuration using a variety of techniques, and considered both strong and weak surface anchoring. After the equilibration process described in Sec. II, we carried out production runs of 60000 steps examining the director configuration every 6000 steps. The general features of the configurations required to assess the overall director structure were essentially time independent. We studied these configurations using the defect-finding algorithm for disclinations described in Ref. [21], and contour plots of the angle of molecular orientation with respect to the director. To apply the defect-finding algorithm we divided the system into a $6 \times 6 \times 6$ lattice of cubic bins (the size is chosen so that the defects ultimately found have a core size of one bin). Note that the creation of a lattice is strictly for convenience in defect finding; the time evolution of the system allows for complete translational freedom. Within each bin, the order parameter tensor

$$Q_{\alpha\beta}(\mathbf{x}) = \frac{3}{2} [\hat{\mathbf{u}}_\alpha(\mathbf{x}) \hat{\mathbf{u}}_\beta(\mathbf{x}) - \delta_{\alpha\beta}] \quad (9)$$

was calculated, its largest eigenvalue taken as the local order parameter S and the corresponding eigenvalue as the local director $\hat{\mathbf{n}}$. Topological defects can be located by considering the directors at the corners of a square (one of the faces of a cube) in the three-dimensional lattice. The idea is to track the course of the intersections of these directors with the order parameter sphere (actually the projective plane RP_2) as one moves around the corners of the real-space square. If the first and last points are in different hemispheres then a disclination line is taken to cut through the center of the square, and is oriented perpendicular to the plane of the square.

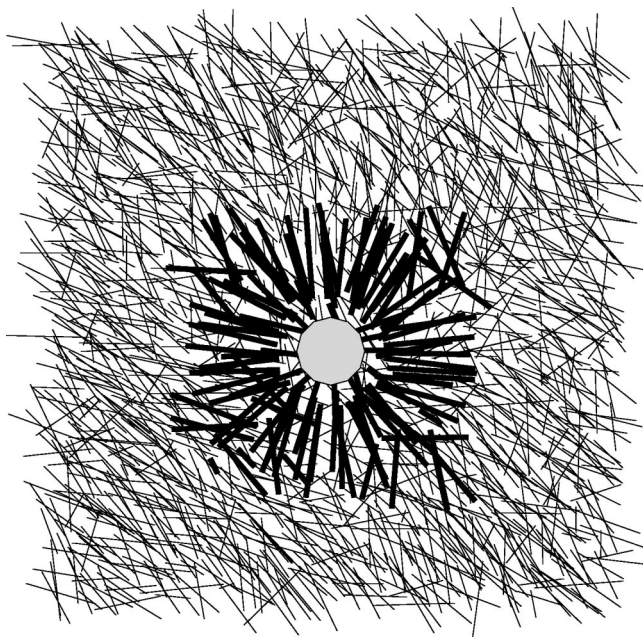


FIG. 3. Molecular configuration for strong anchoring. A subset of the total simulation box centered on the droplet is shown and those molecules closest to the droplet are highlighted to assist in viewing the defect configuration.

For strong anchoring ($W=35000, \xi=0.04$) we detected a Saturn ring configuration using this algorithm (Fig. 2). Given the small size of our droplet this result is consistent with the results of elastic theory [2,3,5,7]. The molecular configuration in the portion of the MD cell surrounding the droplet is shown in Fig. 3, providing a clear view of the strong radial anchoring of the molecules immediately surrounding the sphere. It is clear that the radial anchoring takes place over one molecular layer. Thus it is not possible with our system size to provide more than an estimate of the radius of the

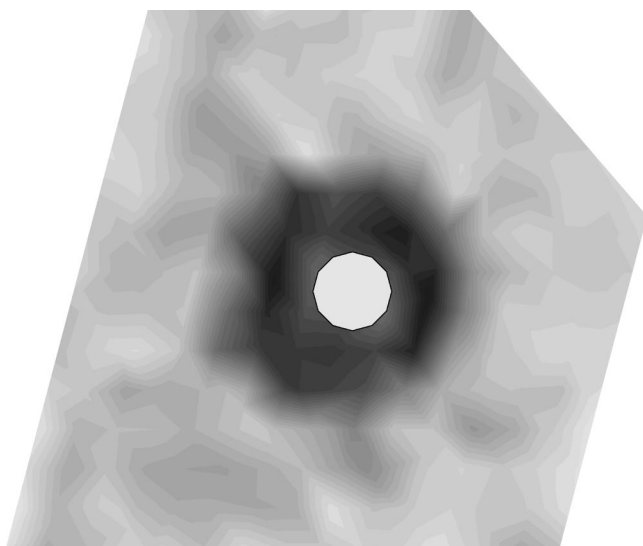


FIG. 4. Contour plot of the director configuration in a slice centered on a droplet with strong radial anchoring. The lighter regions represent molecules aligned with the director, while darker regions indicate molecules perpendicular to the director. Here the director points up out of the page, so the figure shows a Saturn ring in the plane of the figure.

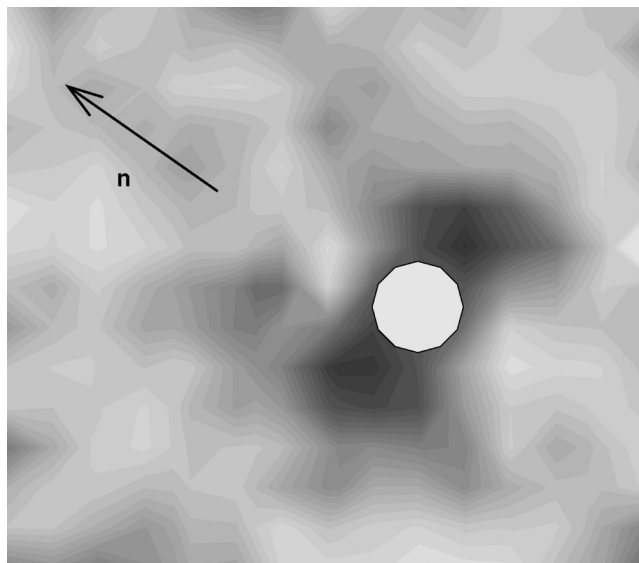


FIG. 5. Contour plot of the director configuration for strong radial anchoring in a slice with the director in the plane of the page as indicated. The lighter regions represent molecules aligned with the director, while darker regions indicate molecules perpendicular to the director.

Saturn ring; that is, it is slightly greater than the radius of the droplet. However, our result is consistent with the results of elastic theory analyses of Refs. [5,22], which found radii of order R . With a larger system size and thus a larger droplet, it should be possible to determine the radius of the ring.

The director configurations can also be visualized using contour plots of the angle of orientation with respect to the director. As shown in Fig. 4 (a slice through the center of the droplet and perpendicular to \hat{n}), the molecular orientation is along the director everywhere except in a ring about the droplet. Figure 5 shows a slice parallel to \hat{n} . Both figures are consistent with the presence of a Saturn ring in the equatorial plane perpendicular to \hat{n} . A similar set of figures for tangential anchoring (Figs. 6 and 7) shows a pair of boojums lo-

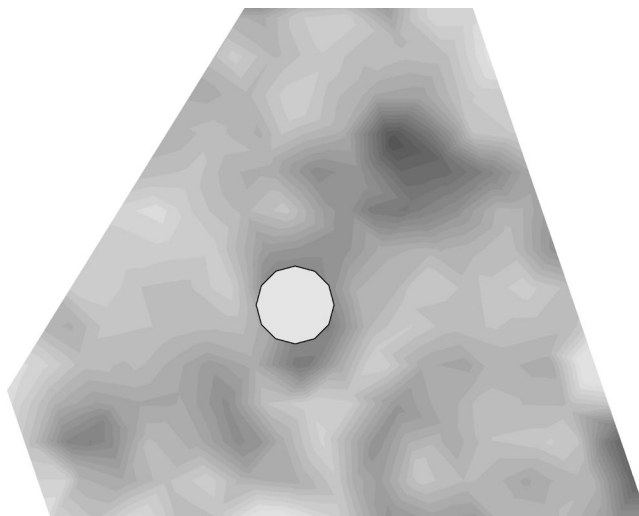


FIG. 6. Contour plot of the director configuration with parallel surface anchoring in a slice perpendicular to the director. Compare with the case of radial anchoring shown in Fig. 4.

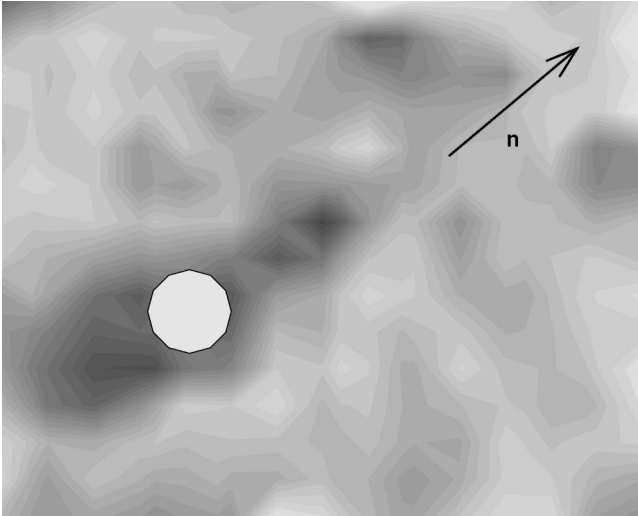


FIG. 7. Contour plot of the director configuration with parallel surface anchoring in a slice in the plane of the director. Compare with the case of radial anchoring shown in Fig. 5.

cated near the poles of the droplet.

For the lower value of the anchoring parameter that we studied ($W=4000$), we found that the Saturn ring is replaced by the surface-ring configuration shown in Fig. 8. This value of W corresponds to a surface extrapolation length $\xi=0.4$, and our result is consistent with the predictions of elastic theory [5,22].

B. Dynamics

To study the dynamics of the immersed droplet, we began with an equilibrated configuration prepared as described at the end of Sec. II. We applied a force to the droplet, and measured its position as a function of time, determining the terminal velocity from the asymptotic slope of the droplet's

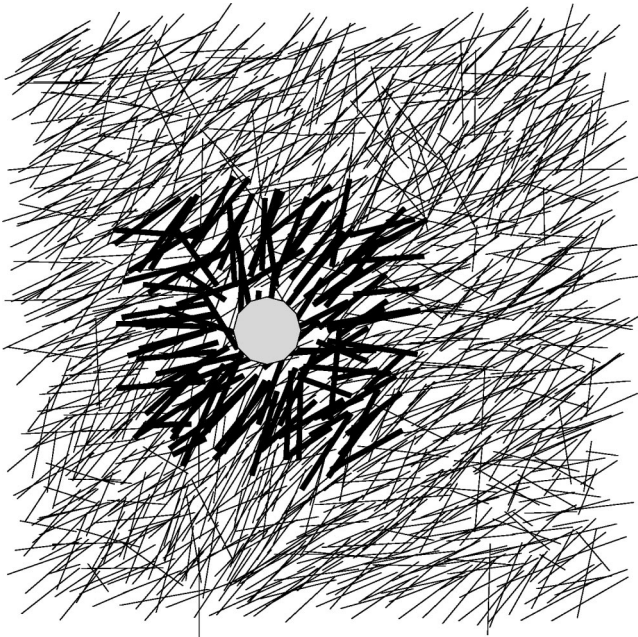


FIG. 8. The same as Fig. 3, but with a weaker radial anchoring ($W=4000$). The Saturn ring has contracted to a surface ring.

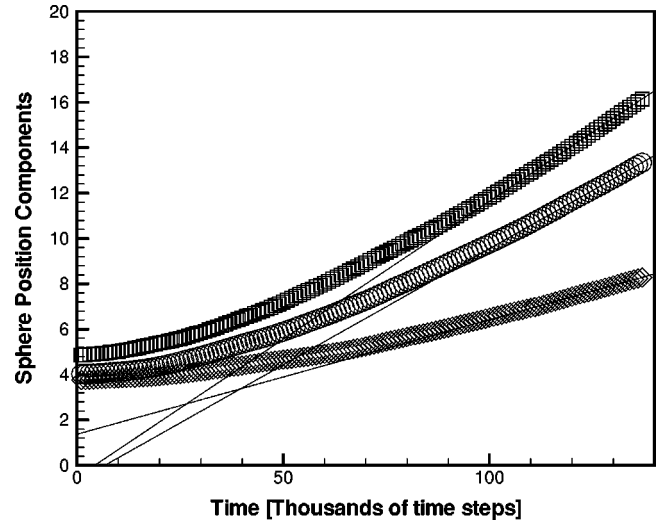


FIG. 9. Illustration of asymptotic velocity measurement. Sphere positions x, y , and z (top to bottom curves, respectively) are shown for a driving force $F=85$ applied at 45° to the director. The positions are measured in units of σ_o . The slopes of the straight lines yield the corresponding asymptotic velocity components v_x , v_y , and v_z .

position as a function of time (see Fig. 9). For a force applied at an angle of 45° with the director, the lift force ratio (the ratio of the components of drag force perpendicular and parallel to the velocity) is given by

$$F_{lift}/F_v = \tan(45^\circ - \theta), \quad (10)$$

where θ is the angle between the terminal velocity vector and the director. The anisotropy of the resistance tensor M is given by

$$M_{\perp}/M_{\parallel} = v_{\parallel}/v_{\perp} = \cot \theta. \quad (11)$$

Table I shows the magnitude of the terminal velocity, the value of θ , the lift force ratio, and the resistance tensor anisotropy for driving forces of different magnitudes for both $W=35000$ (strong anchoring) and for $W=0$. The magni-

TABLE I. Lift force ratio and resistance tensor anisotropy. A force of magnitude F is applied at an angle of 45° to the director and the magnitude v and angle θ (with respect to the director) of the terminal velocity are measured. The lift force ratio F_{lift}/F_v is given by $\tan(45^\circ - \theta)$ and the resistance tensor anisotropy M_{\perp}/M_{\parallel} by $\cot \theta$.

F	v	θ	F_{lift}/F_v	M_{\perp}/M_{\parallel}
$W=35000$				
30	0.09	43.5	0.027	1.06
50	0.12	43.5	0.026	1.05
85	0.17	44.9	0.002	1.00
200	0.24	44.8	0.004	1.01
$W=0$				
5	0.06	37.7	0.128	1.29
20	0.34	44.5	0.009	1.02
40	0.37	42.7	0.041	1.08

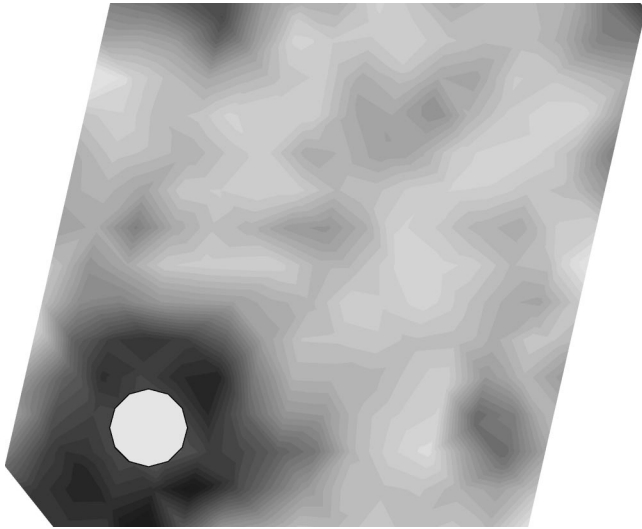


FIG. 10. Slice perpendicular to the director for driving force $F = 250$, with the force applied parallel to the director.

tudes of M_{\perp} and M_{\parallel} in the former case are approximately five times greater than in the latter, as one might expect intuitively. For both cases, the values of θ are generally slightly less than 45° . Thus the lift force ratio is nearly zero, and the resistance anisotropy nearly unity. These results are very different from what was found experimentally and predicted theoretically [4,8] for droplets which are many times larger than the nematic host molecules (the theoretical work

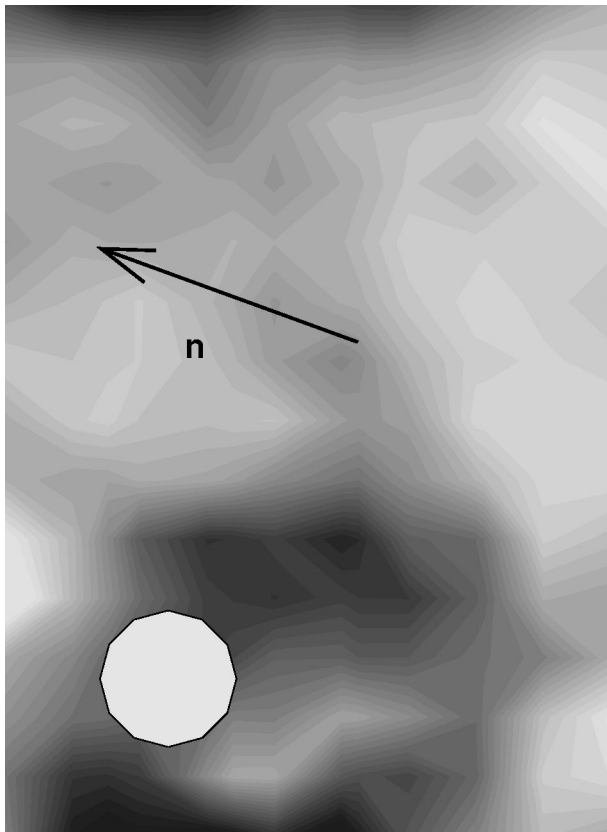


FIG. 11. Slice in the plane of the director for driving force $F = 250$, with the force applied parallel to the director. The Saturn ring is clearly distorted.

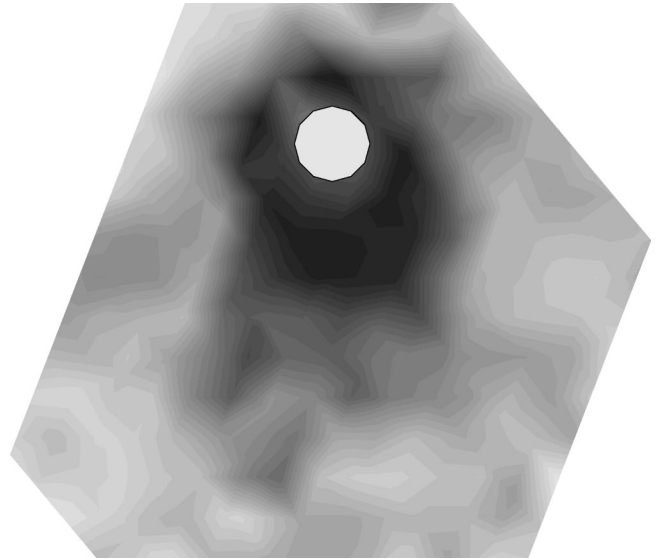


FIG. 12. Slice perpendicular to the director for driving force $F = 250$, with the force applied perpendicular to the director. Again, the Saturn ring is clearly distorted.

uses the Frank elastic energy, and thus assumes large droplets). However, given our small droplet size (diameter equal to the length of a nematic molecule), it is not surprising that the lift force F_{lift} is very small, and the resistance tensor nearly isotropic.

In the anchoring case, there is very little distortion of the Saturn rings for small driving forces. With larger forces, however, the Saturn ring either folds back on itself behind the droplet for parallel driving forces (Figs. 10 and 11) or becomes stretched out behind the droplet while retaining its equatorial position for perpendicular driving forces (Figs. 12 and 13). The distortions become so large that, as one can clearly see in Fig. 11, for example, when the droplet exits the left side of the simulation box and re-enters on the right, it will begin to interact with its own wake. For the no-anchoring case, there is no Saturn ring to distort, but the

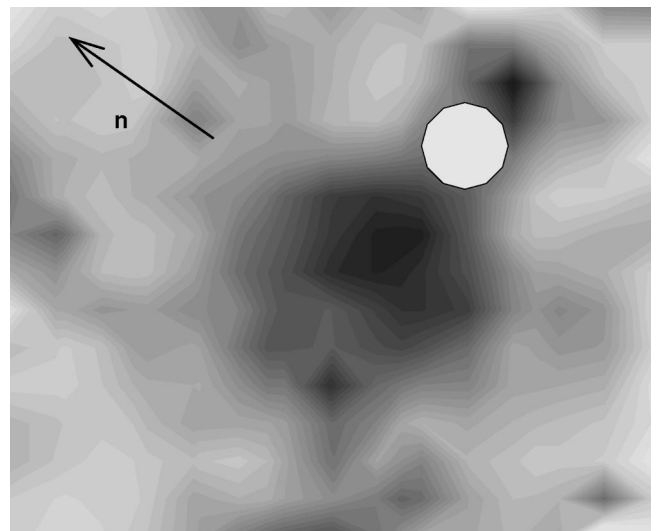


FIG. 13. Slice in the plane of the director for driving force $F = 250$, with the force applied perpendicular to the director.

droplet still causes localized disturbances which eventually result in self-interactions for large driving forces.

IV. CONCLUSIONS

We have shown, in an off-lattice simulation, that, consistent with theoretical predictions, the Saturn ring is the preferred defect configuration around small droplets with radial anchoring embedded in a nematic. We have also shown that lowering the anchoring strength can produce a surface ring instead of a Saturn ring. The Saturn ring increases (compared to the no-anchoring case) resistance to the droplet's motion when the droplet is subjected to a driving force. We found a very small lift force (and correspondingly little anisotropy in the resistance tensor), consistent with the small droplet size studied. Clearly, further work with larger system sizes will allow numerous interesting questions to be studied fruitfully.

The size limitation on the droplet comes, of course, from periodic boundary conditions; if the droplet is too large, the anchoring layers on opposite sides of the droplet will begin to interact with each other. Larger system sizes will also allow an exploration of the variation in Saturn ring radius with particle size and, very importantly, a study of the transition from Saturn ring to dipole. With larger systems, one can also reasonably begin to study multiparticle dispersions.

ACKNOWLEDGMENTS

We are grateful to Professor G. Crawford for helpful discussions. Computational work in support of this research was performed at the Theoretical Physics Computing Facility at Brown University. This work was supported by the National Science Foundation under Grant Nos. DMR-9528092 and DMR98-73849.

-
- [1] P. Poulin, H. Stark, T.C. Lubensky, and D.A. Weitz, *Science* **275**, 1770 (1997).
 - [2] T.C. Lubensky, D. Petey, N. Currier, and H. Stark, *Phys. Rev. E* **57**, 610 (1998).
 - [3] E.M. Terentjev, *Phys. Rev. E* **51**, 1330 (1995).
 - [4] R.W. Ruhwandl and E.M. Terentjev, *Phys. Rev. E* **54**, 5204 (1996).
 - [5] H. Stark, *Eur. Phys. J. B* **10**, 311 (1999).
 - [6] O.V. Kuksenok, R.W. Ruhwandl, S.V. Shiyankovskii, and E.M. Terentjev, *Phys. Rev. E* **54**, 5198 (1996).
 - [7] R.W. Ruhwandl and E.M. Terentjev, *Phys. Rev. E* **56**, 5561 (1997).
 - [8] R.W. Ruhwandl and E.M. Terentjev, *Z. Naturforsch. A* **50a**, 1023 (1995).
 - [9] J.G. Gay and B.J. Berne, *J. Chem. Phys.* **74**, 3316 (1981).
 - [10] For a recent reference, see M.A. Bates and G.B. Luckhurst, *J. Chem. Phys.* **110**, 7087 (1999).
 - [11] D.J. Cleaver, C.M. Care, M.P. Allen, and M.P. Neal, *Phys. Rev. E* **54**, 559 (1996).
 - [12] M.R. Wilson, M.P. Allen, M.A. Warren, A. Sauron, and W. Smith, *J. Comput. Chem.* **18**, 478 (1997).
 - [13] J.L. Billeter, A.M. Smondyrev, G.B. Loriot, and R.A. Pelcovits, *Phys. Rev. E* **60**, 6831 (1999).
 - [14] G.R. Luckhurst, R.A. Stephens, and R.W. Phippen, *Liq. Cryst.* **8**, 451 (1990).
 - [15] R. Berardi, A.P.J. Emerson, and C. Zannoni, *J. Chem. Soc., Faraday Trans.* **89**, 4069 (1993).
 - [16] S. Melchionna, G. Ciccotti, and B.L. Holian, *Mol. Phys.* **78**, 533 (1993).
 - [17] A. Bulgac and M. Adamuți-Trache, *J. Chem. Phys.* **105**, 1131 (1996).
 - [18] S. Nose, *Mol. Phys.* **52**, 255 (1984); W.G. Hoover, *Phys. Rev. A* **31**, 1695 (1985).
 - [19] M. Svanberg, *Mol. Phys.* **92**, 1085 (1997).
 - [20] P. de Gennes and J. Prost, *The Physics of Liquid Crystals* (Clarendon Press, Oxford, 1993).
 - [21] M. Zapotocky, P.M. Goldbart, and N. Goldenfeld, *Phys. Rev. E* **51**, 1216 (1995).
 - [22] R.W. Ruhwandl and E.M. Terentjev, *Phys. Rev. E* **55**, 2958 (1997).